Organic & Biomolecular Chemistry

PAPER

View Article Online
View Journal | View Issue

Cite this: Org. Biomol. Chem., 2019, 17, 9467

Benzochalcogendiazole-based conjugated molecules: investigating the effects of substituents and heteroatom juggling†

Heta A. Patel,‡[a] Viraj J. Bhanvadia,‡[a] Hemant M. Mande,[a] Sanjio S. Zade [b] and Arun L. Patel *[a]

Received 25th August 2019,
Accepted 15th October 2019

DOI: 10.1039/c9ob01762c

rsc.li/obc

A convenient and effective synthetic approach for benzochalcogendiazole-based small molecules has been achieved using polyaniline (PANI)-anchored palladium as a heterogeneous catalyst. The photophysical properties of the synthesized benzochalcogendiazole-based small molecules, having different terminal substituents, have been compared. Moreover, the structural aspects, including the packing patterns and non-bonding interactions of the conjugated molecules, have been investigated using the single crystal X-ray diffraction (SCXRD) technique.

Introduction

Benzochalcogendiazoles such as 2,1,3-benzoxadiazole (BOD), 2,1,3-benzothiadiazole (BTD) and 2,1,3-benzoselenadiazole (BSD) have played an important role as acceptor building blocks[1] in the development of donor–acceptor (D–A) organic conjugated materials for application in organic electronic devices such as organic light emitting diodes,[2] organic field effect transistors,[3,4] and organic solar cells[5] and as dyes.[6] BOD, BTD and BSD-based π-conjugated fluorophores exhibit strong and stable fluorescence along with excellent thermal stabilities.[7] Moreover, BSD-based compounds showed red shifts in their absorption and emission spectra compared with BTD- and BOD-based compounds, because BSD can more effectively lower band gaps.[7a,8] Also, benzoselenadiazoles can effectively tune the optical and electronic properties of the resulting conjugated systems. On the other hand, few studies have proven that benzoxadiazole is a relatively stronger electron acceptor than BTD and BSD due to its larger electron affinity to oxygen.[9] BOD, BTD and BSD are the typical examples, where the optoelectronic properties of the resulting organic conjugated system can be atomistically tuned by single atom substitution.[8b]

The BOD, BTD and BSD derivatives can form well-ordered crystal structures, and the solid-state packing in such molecules strongly depends on intra- and intermolecular S/Se···N interactions and other non-covalent interactions.[10] It is reported that heavier chalcogen (Se) in chalcogenadiazoles show a stronger tendency to form head-to-head dimers. Thus, such non-covalent interactions can be effectively exploited for the formation of supramolecular self-assemblies.[11]

Researchers have utilized the Mizoroki–Heck reaction,[12] Suzuki–Miyaura reaction[13] and Migita–Kosugi–Stille[14] reaction for the synthesis of various benzochalcogendiazole-based conjugated molecules. However, these reactions require costly palladium salts or complexes. Therefore, immobilization of palladium on a solid support for heterogeneous reactions is a cost efficient alternative for these coupling reactions.[15] An important aspect of the development of a heterogeneous catalyst involves the anchoring of the active transition metal salts onto a solid surface. Due to the ability of PANI to easily undergo ion exchange when treated with metal salts and its low solubility in organic solvents and water, this material can be used as a support in heterogeneous catalysis. PANI supported metal ion-based catalysts have been used for many organic transformations such as oxidations,[16] acylations,[17] and coupling reactions,[18] and a few other miscellaneous transformations.[19] In our ongoing research, we have been working on the heterogenization of metal ions on polyaniline (PANI) and its applications in various organic transformations.[20] We also report here the one-pot Wittig–Heck methodology[21] for the construction of a new class of conjugated substituted bis(vinyl arene)-capped benzothiadiazole derivatives. This strategy has several advantages, such as short synthesis without separation and purification of unstable intermediates, minimum waste gene-

[a]Department of Chemistry, Faculty of Science, The Maharaja Sayajirao University of Baroda, Vadodara-390002, India. E-mail: arunpatel_5376@yahoo.co.in
[b]Department of Chemical Sciences, Indian Institute of Science Education and Research (IISER) Kolkata, Mohanpur-741246, India

†Electronic supplementary information (ESI) available: XRD characterization data of catalyst, crystallographic data, spectral data (^{1}H and ^{13}C NMR, mass, and HRMS), and CIF files. CCDC 1876836, 1850340, 1850346, 1850348, 1876837, 1850345, 1850341 and 1850342. For ESI and crystallographic data in CIF or other electronic format see DOI: 10.1039/c9ob01762c

‡These authors have contributed equally to this article.

ration, and judicious utilization of time and resources.[22] Apart from a few recent reports, benzochalcogendiazole-based substituted vinyl arenes have not been explored much.[5a,23]

In the present paper, benzochalcogendiazole-based small conjugated molecules are synthesized by the Suzuki–Miyaura reaction with phenyl and thiophene boronic acid (06 examples) as well as by the Mizoroki–Heck reaction with styrene, 4-methylstyrene and vinylpyridine (07 examples) using palladium immobilized on the polyaniline (PANI) solid support as a cost-efficient heterogeneous catalyst. The molecules synthesized by the Suzuki–Miyaura reaction and Mizoroki–Heck reaction are designed and studied to obtain very effective and useful information about the photophysical and structural effects arising from the heteroatom juggling (O/S/Se) in the benzochalcogendiazole unit. Using the one-pot Wittig–Heck methodology, we have synthesized conjugated bis(vinyl arene)-capped benzothiadiazole derivatives, by varying different substituted aldehydes from electron releasing (–OCH_3, 1,3-dioxolyl, –CH_3) to electron withdrawing (–Cl, –F, –CN, –NO_2) groups using the heterogenous catalyst PANI-Pd, which are further tested for the effects of substitution on their photophysical properties.

Results and discussion

Synthesis

Polyaniline (PANI) was prepared from aniline hydrochloride by a chemical oxidation protocol using ammonium persulfate followed by neutralization with aqueous ammonia.[24] Palladium was immobilized on the sample of PANI by treating it with a solution of $PdCl_2$ in acetonitrile. The catalyst PANI-Pd was characterized by XRD, BET and ICP-AES.[20a] Two signals at 2θ values of 40° and 46° in the X-ray diffraction (XRD) analysis indicate the presence of Pd ions (Fig. S1†). ICP-AES analysis of the catalyst sample indicates a 3.86% loading of palladium metal.[20a]

The catalyst system was applied for the Suzuki–Miyaura coupling reaction. The standard reaction conditions are shown in Scheme 1, where dibromobenzochalcogendiazoles **1–3** were treated with phenyl/thiophene boronic acid in the presence of the PANI-Pd catalyst and K_2CO_3 as a base. The biaryl products **7–9** were isolated in high yields and characterized by spectroscopic techniques.

The PANI-Pd catalyst was further explored for the standard Mizoroki–Heck coupling reaction. The dibromobenzochalcogendiazoles **1–3** were subjected to the Mizoroki–Heck coupling reaction with vinyl arenes **10–12** in the presence of the PANI-Pd catalyst and a mild base, K_2CO_3 (Scheme 2). Products **13–19** of the Mizoroki–Heck reaction were obtained in good yields and isolated as the *E*-isomer as shown in Scheme 2. All the synthesized compounds were characterized by the usual spectroscopic techniques.

Many substituted vinyl arenes are costly, not readily available, and tend to polymerize at a higher temperature. Here, a one-pot Wittig–Heck reaction methodology was adopted to overcome these difficulties.[20a] Vinyl arenes were prepared *in situ* by the Wittig reaction of an aldehyde and Ph_3PCH_3I and then subjected to the Mizoroki–Heck reaction (Fig. 1). The easy availability of aromatic aldehydes compared to the substituted vinyl arenes makes the one-pot methodology more favourable for the construction of bis(vinylarene)-capped benzochalcogendiazoles. A series of substituted benzaldehydes having different electron releasing/withdrawing groups were used to form substituted vinyl arenes *in situ*, which subsequently reacted with 4,7-dibromo-2,1,3-benzochalcogendiazole in the presence of PANI-Pd catalysts affording the final products in a single pot (Scheme 3).

Since the Wittig reaction was performed with aromatic aldehydes and Ph_3PCH_3I, the intermediate vinyl arenes immediately underwent the Mizoroki–Heck reaction with aryl halides

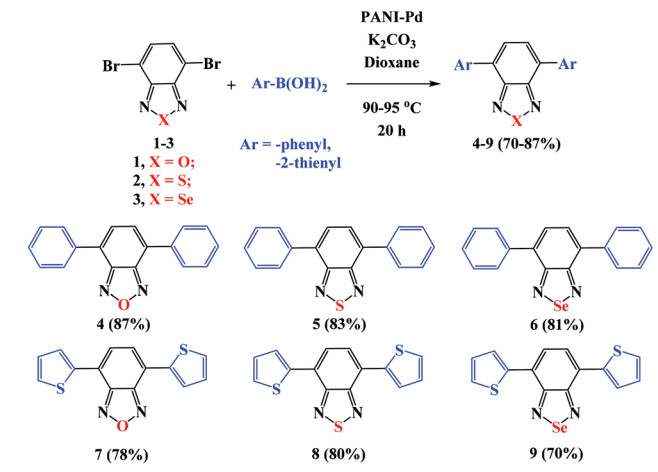

Scheme 1 PANI-Pd catalyzed Suzuki–Miyaura reaction.

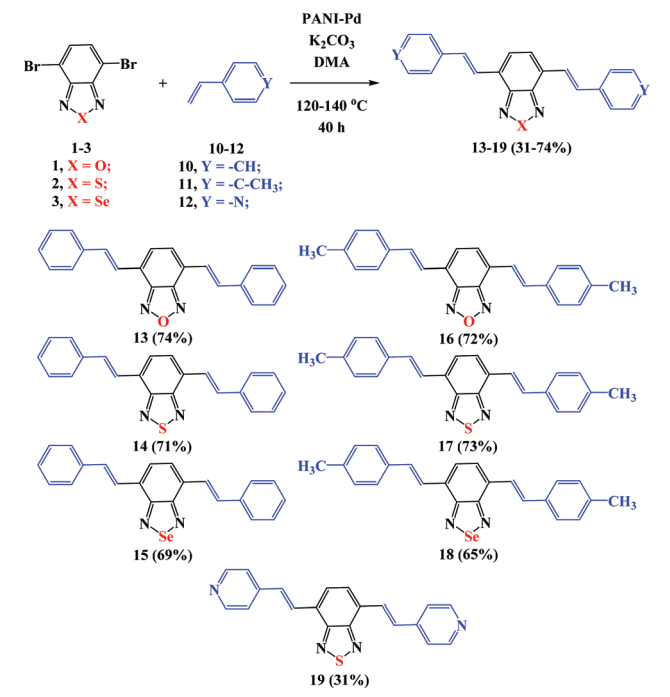

Scheme 2 PANI-Pd catalyzed Mizoroki–Heck reaction.

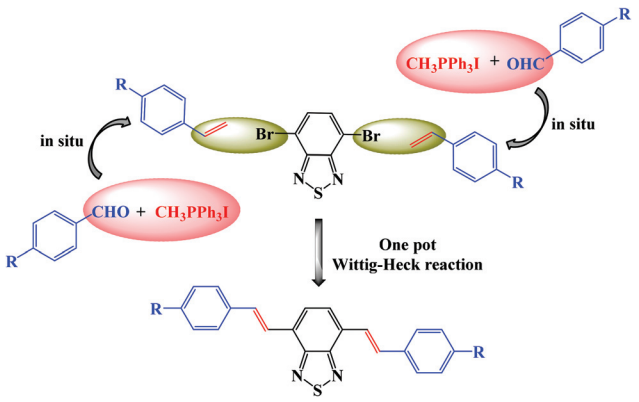

Fig. 1 One-pot Wittig–Heck approach.

in the presence of PANI-Pd. Their stereochemistry is determined in the second step, which favours the formation of the *E*-isomer. A series of compounds **14**, **17**, and **20–25** were synthesized and isolated in good yields (56–71%) as shown in Scheme 3.

Photophysical studies

The absorption and emission spectra of all the compounds were studied in chloroform solution. The absorption spectra of compounds **4–9** exhibit absorption bands between 300 and 550 nm which are assigned to $\pi \rightarrow \pi^*$ and charge transfer (CT) transitions (Fig. 2a). The absorption spectra of compounds **7–9** were red-shifted compared to compounds **4–6** owing to the planar structures of **7–9** and the presence of more electron donating thienyl groups compared to the phenyl groups. The emission spectra of compounds **4–9** (Fig. 2b) exhibited emission maxima between 484 and 620 nm with Stokes shift values in the range of 102–140 nm (Table 1). Compound **4** showed emission maximum at 484 nm, whereas compound **9** showed emission maximum at 620 nm, exhibiting a red-shift of 136 nm. It is noteworthy that compounds **4** and **5** exhibited a single higher energy emission band, while compound **6** showed relatively red shifted typical broad CT emission at 514 nm. However, replacement of the terminal phenyl group with a thienyl group resulted in a red shift of emission maxima as well as dual band emission for compounds **7** and **8** while compound **9** showed much red shifted typical broad CT emission at 620 nm.

The photophysical properties of compounds **13–19** were studied by UV-visible spectroscopy in chloroform solutions (Fig. 3a). Compounds **13–19** exhibit a characteristic dual band nature, and the higher energy bands (250–350 nm) can be ascribed to the $\pi \rightarrow \pi^*$ transition of the conjugated backbone, while the lower energy bands correspond to the charge transfer transitions (Fig. 3a). Introduction of a vinyl spacer between the central BOD/BTD/BSD unit and the terminal phenyl group resulted in the bathochromic shifting of the absorption maxima as well as lowering of the optical band-gaps of compounds **13–15** compared to those of compounds **4–6**. Moreover, the effect of the presence of the electron donating substituent (methyl group) has been established by the bathochromic shift of the absorption maxima (λ_{max}^{abs}) of compounds

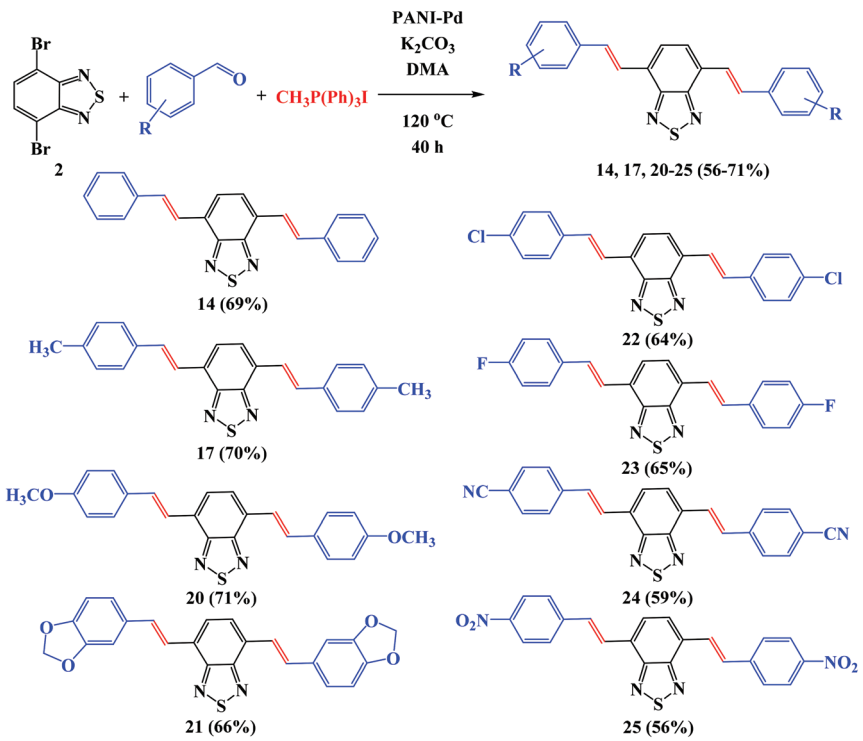

Scheme 3 PANI-Pd catalyzed one-pot Wittig–Heck reaction.

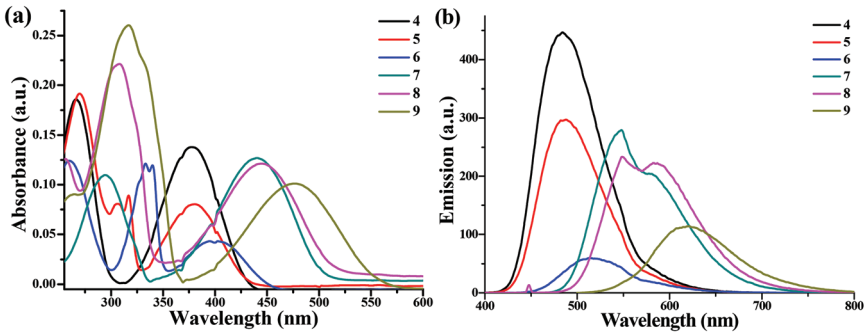

Fig. 2 (a) Absorption spectra and (b) emission spectra of compounds **4–9** in chloroform solution (10^{-5} M).

Table 1 Photophysical properties of synthesized benzochalcogendiazole-based conjugated molecules (compounds **4–9** and **13–25**); literature values are given in the parentheses

Sr. no	Compounds	λ_{max}^{abs} (nm)	λ_{max}^{em} (nm)	λ_{onset} (nm)	Stokes shifts (nm)	Log ε	E_g^{opt} (eV)
1	**4**	266, 378	484	444	106	4.14	2.79
2	**5**	269, 316, 380(380)[27]	488(490)[27]	456	108	3.90	2.72
3	**6**	260, 333, 399(408)[28]	514(505)[28]	480	113	3.63	2.58
4	**7**	294, 440(441)[14]	548, 581	506	108	4.10	2.45
5	**8**	255, 307, 447(466)[29]	549, 582	521	102	4.08	2.38
6	**9**	262, 317, 480(478)[28]	620(597)[28]	555	140	4.00	2.23
7	**13**	318, 444	548, 578	506	104	4.48	2.45
8	**14**	329, 449	548(552),[23a] 583	520	99	4.25	2.34
9	**15**	310, 338, 451	549, 588	540	134	3.80	2.30
10	**16**	322, 453	549, 583	534	90	4.49	2.32
11	**17**	329, 459	552, 591	536	132	4.50	2.25
12	**18**	343, 489	624	582	135	4.11	2.13
13	**19**	329(329),[5a] 421(428)[5a]	521(510)[5a]	479	100	4.34	2.59
14	**20**	330(326),[23b] 472(460)[23b]	554, 601(595)[23b]	555	129	4.30	2.16
15	**21**	323, 460	554, 596	568	136	4.28	2.14
16	**22**	328, 445	543, 582	527	98	4.32	2.31
17	**23**	328, 448	547, 582	523	98	4.28	2.32
18	**24**	333, 440	529	503	88	4.47	2.48
19	**25**	331, 376, 446	513, 533	516	67	4.37	2.39

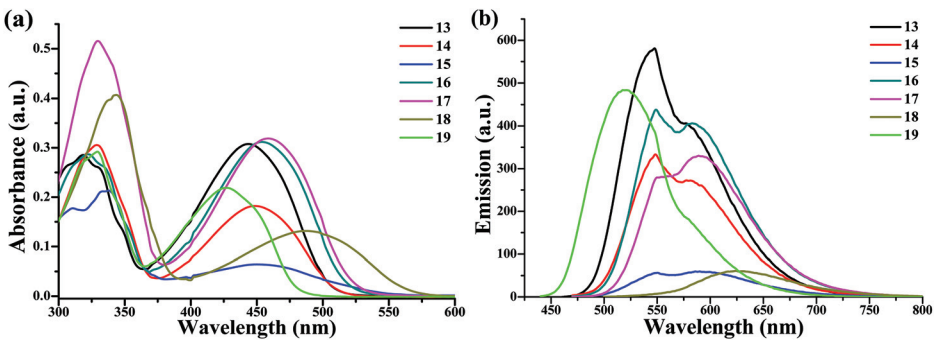

Fig. 3 (a) Absorption spectra and (b) emission spectra of compounds **13–19** in chloroform solution (10^{-5} M).

16–18 compared to those of compounds **13–15** (see Table 1). The steady-state fluorescence spectroscopy of compounds **13–19** showed that the emission maxima (λ_{max}^{em}) varied in the range of 103 nm, that is, from 521 nm for compound **19** to 624 nm for compound **18** and the corresponding Stokes shift values range between 90 and 135 as shown in Fig. 3b and Table 1.

Also, the effects of the insertion of vinyl spacers were evidenced by the dual band emission spectra of compounds **13–15** (Fig. 3b) compared to those observed for compounds **4–6** (Fig. 2b). Also, compounds **16** and **17** exhibited dual band emission spectra (Fig. 3b). Compound **18** with a central BSD-unit showed a much less intense and red shifted typical broad CT band at 624 nm. Compound **19**, with electron withdrawing

terminal pyridyl units, exhibited blue shifted emission at 521 nm.

From the absorption and emission spectra of **4–18**, we observed that λ_{max}^{abs} and λ_{max}^{em} exhibited a bathochromic shift when heavier chalcogen atoms were introduced into the benzochalcogendiazole unit. This could be attributed to the increase in the electron density and atomic radius of the heteroatom (from oxygen to selenium) resulting in an improved intramolecular charge transfer (ICT).[9c] Apart from this, decreased $\log \varepsilon$ values of BSD-based compounds (compounds **6**, **9**, **15** and **18**; Fig. 2a and 3a) compared to those of the BTD and BOD-based compounds (compounds **4**, **5**, **7**, **8**, **13**, **14**, **16** and **17**) can be ascribed to the decrease in the electronegativity of the heteroatom and increased size of the atom, as moving from oxygen to sulphur to selenium.[4b] The presence of a larger selenium atom reduces the oscillator strength for S_0 to S_1 transitions drastically, which in turn results in reduced $\log \varepsilon$ values.[25] Selenium derivatives (compounds **6**, **9**, **15** and **18**) exhibited relatively large Stokes shifts compared to their corresponding oxygen and sulphur derivatives, which can be ascribed to the dipole–dipole interactions owing to the generation of a polar excited state, thereby giving rise to typical broad CT emissions.[5a]

Compounds synthesized by the one-pot Wittig–Heck reaction were studied for their photophysical properties by UV-visible spectroscopy and steady-state fluorescence spectroscopy in chloroform solutions (Fig. 4a and b and Fig. S2†). As shown in Fig. 4a, compound **20** with an electron releasing methoxy group shows absorption maxima (λ_{max}^{abs}) at 472 nm whereas compound **24** with an electron withdrawing cyano group shows absorption maxima (λ_{max}^{abs}) at 440 nm, exhibiting a blue shift of 32 nm as shown in Table 1. Steady-state fluorescence studies of compounds **14**, **17**, and **20–25** showed dual emission band spectra and the λ_{max}^{em} for the compounds varied in the range of 88 nm, that is, from 513 nm for compound **25** which has an electron-withdrawing nitro group to 601 nm for compound **20** with an electron-releasing methoxy group as shown in Fig. 4b and Table 1, exhibiting a red shift of the emission maxima while moving from compounds with electron withdrawing to electron releasing substituents. Moreover, the dual band emission spectra of compounds **7**, **8**, **13–17** and **20–23** (Fig. 2b, 3b and 4b) can be ascribed to the vibronic progression due to distinct transitions associated with typical C–C stretching motions within the rigid conjugated structure and the energy difference between these two emissions ranges between 0.12 and 0.16 eV.[26]

The interaction of the basic nitrogen of terminal pyridine units with mineral acid is also studied as protonation results in significantly altered absorption and emission characteristics. Compound **19** was spectroscopically studied for its protonation behavior. The absorption spectrum of compound **19** exhibited strong absorption in the range of 280–500 nm, whereas the first absorption band near 300 nm can be assigned to $\pi \rightarrow \pi^*$ electronic transitions and the second absorption band near 450 nm can be attributed to charge transfer transition. Upon addition of dilute methanolic HCl (0.2 mL; 0.625 mM solution), the intensity of the first absorption band at 326 nm decreases and shifts to 331 nm, while that of the second band at 421 nm increases and shifts to 427 nm as shown in Fig. 5.

The emission spectrum of compound **19** exhibited strong emission at 521 nm upon excitation at 421 nm as shown in Fig. 5b, which shifts to 483 nm with an additional shoulder peak at 509 nm after protonation. In other words, the fluorescence of compound **19** in the neutral state is quenched upon addition of an acid. Quenching is observed in the presence of dilute HCl and is regenerated by the addition of ammonia, making the process reversible, which can be attributed to the protonation–deprotonation process of the terminal pyridine groups, allowing reversible inter-conversion between the cationic and neutral forms of compound **19**.

Single crystal X-ray diffraction (SCXRD) analysis

Suitable single crystals of compounds **13–15**, **18**, **19**, **21** and **23** were obtained by slow evaporation of the saturated solution in petroleum ether/chloroform of the corresponding compounds. The thermal ellipsoid plots (at 50% probability) for each crystal structure are given in the ESI (Fig. S3–S10†). Crystallographic data and structure refinement parameters are listed in Table S1† in the ESI. A single crystal X-ray study confirmed the *E*,*E*-orientations along the vinyl group (Fig. 6) and revealed important information about the heteroatom (O, S and

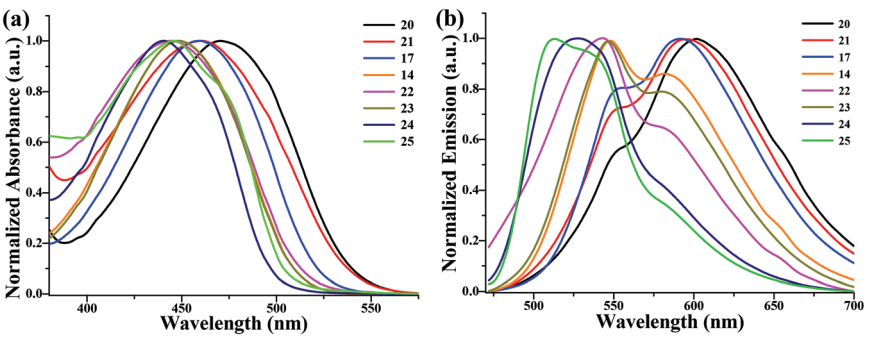

Fig. 4 Normalized (a) absorption and (b) emission spectra of benzothiadiazole-based conjugated molecules (compounds **14**, **17**, **20–25**) in chloroform solution (10^{-5} M).

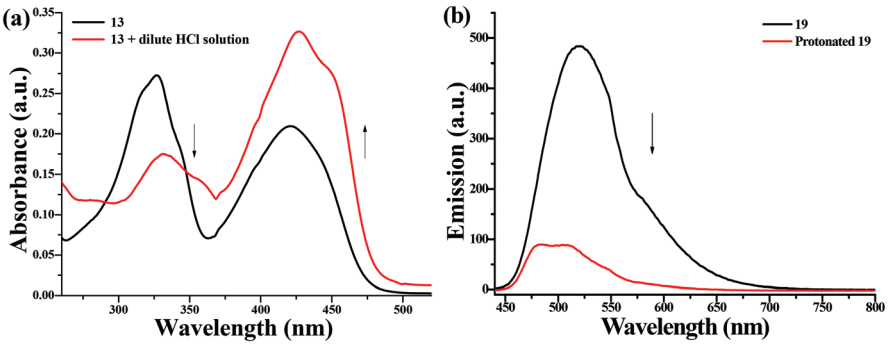

Fig. 5 (a) Absorption and (b) emission spectra of compound **19** before and after the addition of methanolic HCl.

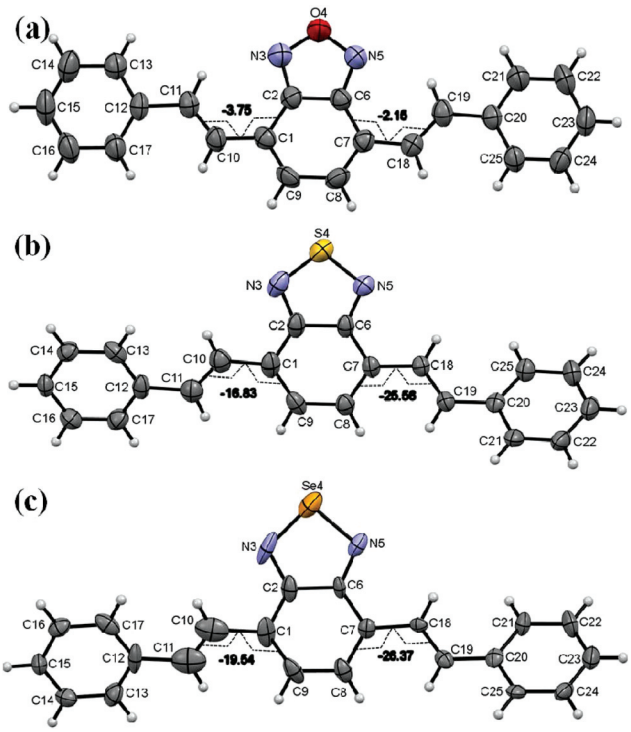

Fig. 6 ORTEP diagram of crystal structures of compounds (a) **13**, (b) **14** and (c) **15**; ellipsoids are at 50% thermal probability.

Se) juggling in compounds **13–15**. However, orientation of the styryl group with respect to the chalcogendiazole ring is different for compound **13** compared to compounds **14** and **15**. Compounds **13–15** crystallize in a monoclinic crystal system with the space group *Pn* for **13** and $P2_1/c$ for **14** and **15**. The crystal structure of compound **13** is almost coplanar (see Table S2†), whereas the styryl groups in **14** and **15** deviate significantly from the central BTD and BSD units (Fig. 6b and c). Similarly, compounds **13–15** showed distinct variations in bond angles N–O–N (111.40°), N–S–N (100.60°) and N–Se–N (94.68°) for five-membered benzochalcogendiazole rings. The effects of heteroatom juggling in compounds **13–15** are also pronounced in terms of crystal packing.

Compound **13** is packed as a layered structure with slip-stacked parallel 1-D chains with π–π stacking (3.39 Å; Fig. 7a and b, Fig. S11a†). Compound **14** shows C–H···π interaction (2.85 Å, between carbon C22 and hydrogen H17; Fig. S11b†) promoted crystal packing with a 2-D interlocking pattern (Fig. S11c†). Moreover, the central BTD units of the adjacent molecules are oppositely cross-aligned with a distance of 3.72 Å. The absence of effective π–π stacking can be ascribed to the increased torsional angles (Table S2†). Also, as an effect of reduced planarity, the log ε value of compound **14** (4.25, see Table 1) is much lower compared to that of compound **13**.

Furthermore, the replacement of S with Se within the five-membered benzochalcogendiazole rings increased the torsion angles in compound **15** (Fig. 6c and Table S2†). Compound **15** exhibited C–H···π interaction (2.81 Å, between carbons C23

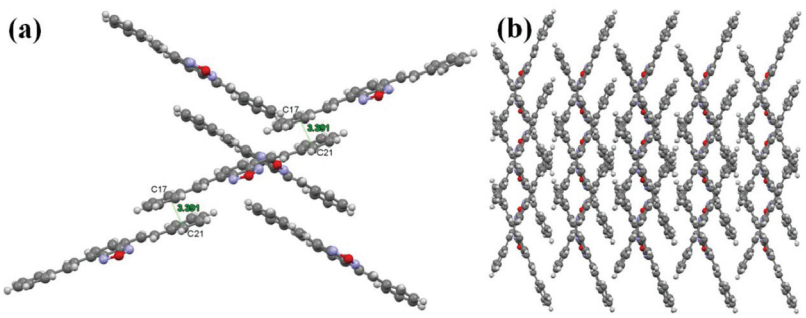

Fig. 7 (a) π–π stacking between the molecules of compound **13**; (b) herringbone type crystal packing of compound **13** along the *ac*-axis.

and C24 and hydrogen H13) and Se···Se interaction (3.78 Å) promoted crystal packing with a 2-D interlocking pattern (Fig. S11d and e†). Moreover, the central BSD units of the adjacent molecules are oppositely cross-aligned with a shorter distance of 3.67 Å, compared to that of 3.72 Å for compound **14**, owing to an additional Se···Se non-bonding interaction (Fig. S11d†). Again, the absence of effective π–π stacking and loss of planarity within the molecules further decreased the log ε value of compound **15** (3.80, see Table 1) compared to that of compounds **13** and **14**.

Introduction of the *p*-methyl substituent on terminal phenyl rings substantially decreased the torsional angles in compound **18** (Fig. 8a and Table S2†). Compared to compound **15**, compound **18** exhibited significant numbers of non-bonding interactions involving C–H···π (ranging from 2.78 to 2.88 Å), C–H···Se (3.05 Å; between selenium Se4 and hydrogen H38), Se···N (ranging from 3.00 to 3.43 Å) and Se···Se (3.79 Å) interactions. In the crystal structure of compound **18**, four molecules of **18** form 3 pairs of Se···N interactions, which are further connected to the dimer *via* Se···N interactions (Fig. S11f†). These extended 1-D Se···N interactions form a hexagonal 1-D array of the molecules which are closely packed to form a rotating mill like structure (Fig. 8b).

Introduction of the 1,3-dioxolyl substituent on both the terminal phenyl rings (compound **21**) decreased the torsional angles (Fig. 9 and Table S2†).

Compound **21** exhibited π–π stacking (3.39 Å; between carbons C20 and C20 of two adjacent benzo[*d*][1,3]dioxol-5-yl rings), C–H···π interaction (2.76 Å; between carbon C20 and hydrogen H20) and N–H hydrogen bonding (2.70 Å; between nitrogen N5 and hydrogen H16B) promoted crystal packing with a 2-D rectangular arrangement of molecules along the *c*-axis (Fig. S12a and b†). Compound **21** showed an increased

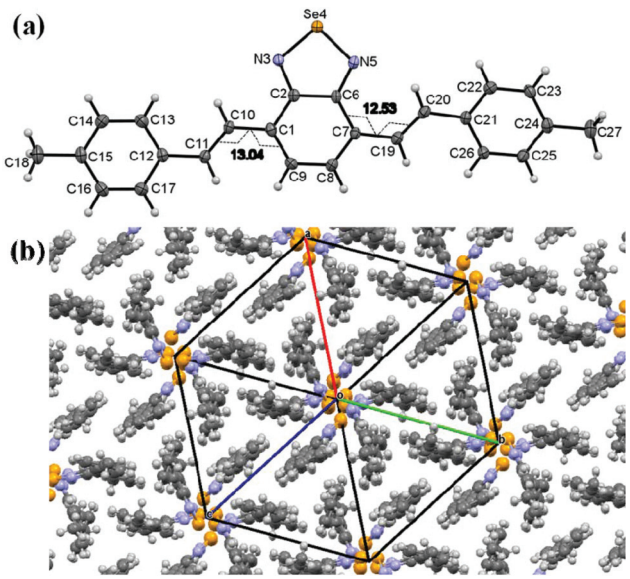

Fig. 8 (a) ORTEP diagram of the crystal structure of compound **18**; ellipsoids are at 50% thermal probability; (b) clock-wise rotating mill like crystal packing of compound **18** along the *abc*-axis.

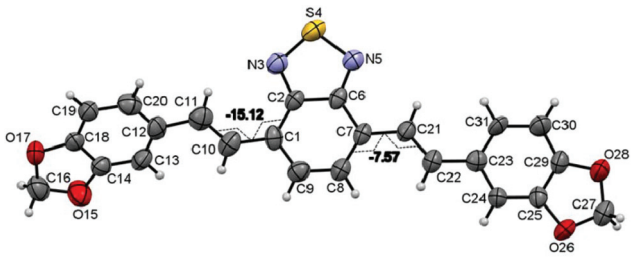

Fig. 9 ORTEP diagram of the crystal structure of compound **21**; ellipsoids are at 50% thermal probability.

log ε value (4.28) compared to that of 4.25 for compound **14** which can be ascribed to the effective π–π stacking as well as improved planarity of the molecule.

Introduction of a smaller and electronegative fluorine atom as the substituent resulted in increased torsional angles (Fig. 10a and Table S2†). Compound **23** showed π–π stacking (3.39 Å; between two oppositely cross-aligned BTD units), C–H···π interaction (2.77 Å; between carbons C19 and C20 and hydrogen H23) and F–H hydrogen bonding (2.64 Å; between fluorine F27 and hydrogen H14 as well as 2.64 Å; between fluorine F18 and hydrogen H13; Fig. S12d†). Apart from these, compound **23** exhibited supramolecular bifurcated S···F interactions between fluorines F18 and F27 and sulphur S4 of the central BTD unit (3.12 Å and 3.06 Å, respectively) forming a 1-D ribbon-like structure along the *ab*-axis (Fig. 10b). Compound **23** showed crystal packing with a 2-D interlocking pattern along the *c*-axis (Fig. S12c†).

Apart from BTD-based molecules containing terminal phenyl and substituted phenyl rings, compound **19** with terminal pyridine rings was also synthesized and the study of its crystal structure revealed that the molecule is relatively planar with decreased torsional angles (Fig. 11a and Table S2†).

Moreover, a molecule of water is trapped between two adjacent molecules, exhibiting non-bonding N···O interaction (2.93 Å; between nitrogen N45 and oxygen O1), N–H hydrogen bonding (2.12 Å; between nitrogen N37 and hydrogen H1B and 2.16 Å; between nitrogen N45 and hydrogen H1A), and O–H hydrogen bonding (2.60 Å; between oxygen O1 and hydrogen H18) as well as non-bonding C···H interactions (2.90 Å and 2.80 Å, respectively, between hydrogens H1A and H1B and carbons C38 and C46) (Fig. S13†). Also, the crystal structure of compound **19** exhibited N–H hydrogen bonding (2.69 Å; between nitrogen N12 and hydrogen H33) and non-bonding N···S interactions (3.35 Å; between nitrogen N12 and sulphur S29), depicted in Fig. S13.† As shown in Fig. 11b, compound **19** showed strong π–π stacking (3.29 Å; between carbons C16 and C24 of the adjacent molecules with oppositely cross-aligned central BTD-units) and C–H···π interaction (2.89 Å; between hydrogen H24 and carbon C49). The improved planarity and effective π–π stacking between the adjacent molecules can also be correlated with the improved absorptivity (with a log ε value of 4.34) compared to that of compound **14** (with a log ε value of 4.25).

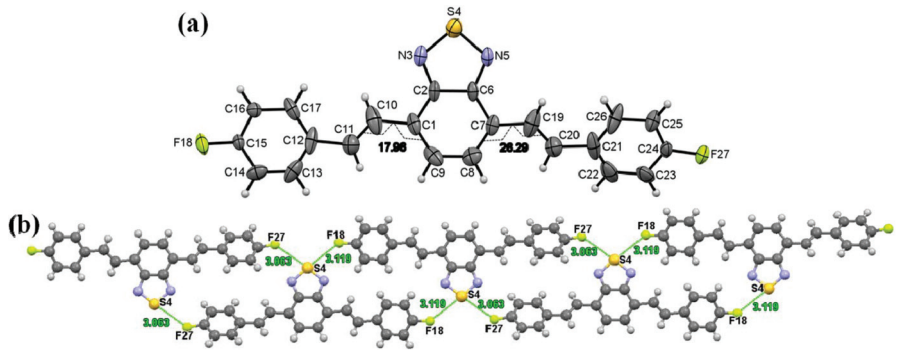

Fig. 10 (a) ORTEP diagram of the crystal structure of compound **23**; ellipsoids are at 50% thermal probability; (b) 1-D ribbon like crystal packing of compound **23** along the *ab*-axis.

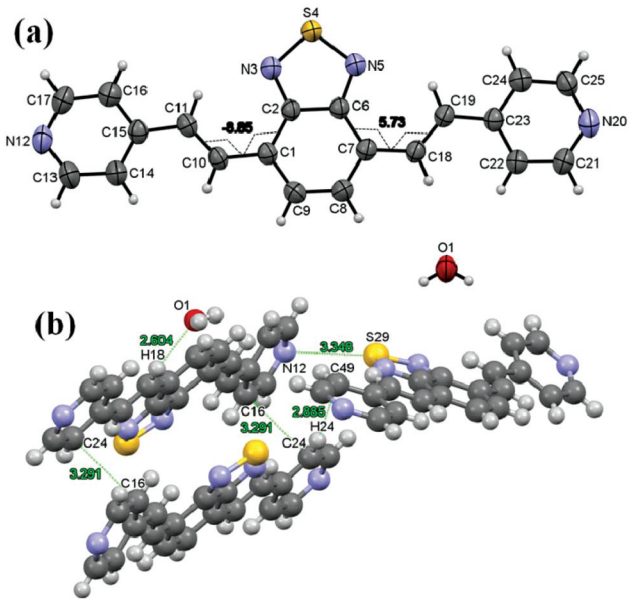

Fig. 11 (a) ORTEP diagram of the crystal structure of compound **19**; ellipsoids are at 50% thermal probability; (b) π–π stacking, C–H···π interaction and non-bonding N···S interaction promoted crystal packing of compound **19**.

Carboxylic acid–pyridine carboxamide combinations are one of the well-known and well-established co-crystal forming systems.[30] Hydrogen bonding of carboxylic acids with molecules having basic functional groups, such as 4,4′-bipyridine, phenazine, 2-pyridone, and isonicotinamide, results in recognition *via* an acid···pyridine heterosynthon instead of a carboxylic acid dimer.[31] Co-crystal strategies underline the self-assembly of functional compounds which may yield a new generation of multidimensional supramolecular networks due to various intermolecular interactions (hydrogen bonding, π–π stacking interaction, anion–π interaction *etc.*).[32]

The co-crystals were prepared through solution crystallization experiments, by mixing the corresponding reactants in a 1 : 1 molar ratio (compound **19** and terephthalic acid) in a hot methanolic solution for 30 minutes.

The product was filtered and recrystallized in dimethyl sulphoxide (DMSO) to obtain co-crystals as needle-like orange crystals. It was observed that within the co-crystals, a terephthalic acid unit links two adjacent terminal pyridine units of compound **19** *via* pyridine carboxamide salt formation (Fig. 12a), which results in substantially reduced torsional angles compared to those of compound **19** which shows that

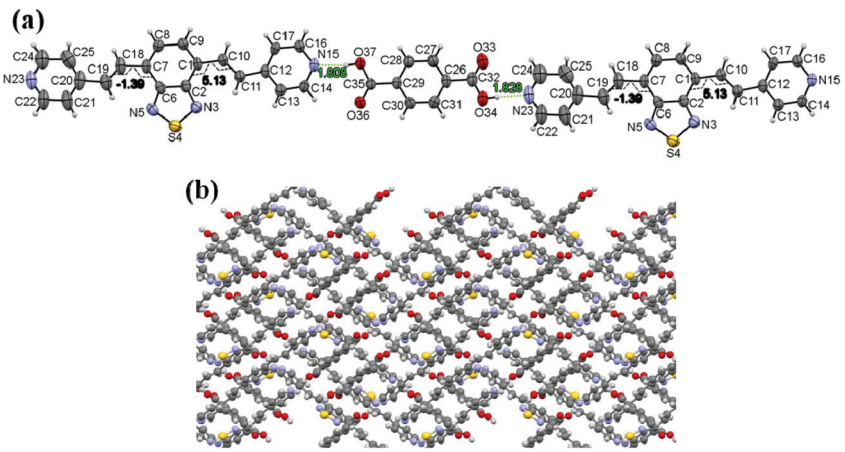

Fig. 12 (a) Hydrogen bonding interactions between the terminal pyridine units of **19** and terephthalic acid units; (b) herringbone type crystal packing of the co-crystal along the *a*-axis.

after the formation of the co-crystals the molecule has become essentially flat (Table S2†). The co-crystals exhibit O–H bonding (ranging from 2.40 to 2.69 Å; Fig. S14c†) resulting in a 1-D polymeric array (Fig. 12a) of alternate molecules of terephthalic acid and compound **19**. These 1-D polymeric arrays are π-stacked to form a layered structure, packed together *via* S–H and O–H interactions. Moreover, the co-crystals showed π–π stacking between the terminal pyridine ring, carbon C13 and terephthalic acid, carbon C26 (3.37 Å; Fig. S14b†) as well as between two adjacent terephthalic acid units, carbons C31 and C29 (3.40 Å; Fig. S14b†). Such types of molecules are potentially good candidates for applications in organic field effect transistors.

Conclusion

We report here the synthesis of various benzochalcogendiazole-based π-conjugated fluorescent molecules using the heterogeneous Pd anchored PANI catalyzed Suzuki–Miyaura reaction, Mizoroki–Heck reaction and one-pot Wittig–Heck reaction. The one-pot Wittig–Heck methodology provided benzothiadiazole-based conjugated fluorescent molecules having electron releasing as well as electron withdrawing substituents. All the synthesized benzochalcogendiazole-based conjugated molecules were characterized by ^{1}H and ^{13}C NMR spectroscopy as well as by high resolution mass spectrometric (HRMS) analysis. The synthesized conjugated molecules were studied for their photophysical properties by UV-visible and steady-state fluorescence spectroscopy. The UV-visible and steady state fluorescence spectra of the phenyl- and thiophene-capped benzochalcogendiazole derivatives (compounds **4–9**) and bis(vinyl arene)-capped benzochalcogendiazole derivatives (compounds **13–18**) exhibited a bathochromic shift of the absorption and emission maxima as a result of heteroatom juggling (O/S/Se) within the central benzochalcogendiazole unit. Moreover, bis(vinyl arene)-capped benzothiadiazole derivatives (compounds **14**, **17**, **20–25**), obtained *via* the one-pot Wittig–Heck reaction, exhibited a blue shift as the substituents on the terminal phenyl rings varied from electron releasing to electron withdrawing groups, owing to the distinctive –R group effect. A single crystal X-ray diffraction study revealed the *trans* orientation of the vinyl linkage between the phenyl and BOD/BSD/BTD units. The molecules showed significant non-conventional interactions such as π–π, N–H, CH–F, S–F, Se–Se, Se–N and CH–π interactions, which are in agreement with the different crystal packing and orientation of the substituted phenyl ring with respect to the central unit. The co-crystal of terephthalic acid and compound **19** was found to be an essentially flat molecule which can be a good candidate for application in organic field effect transistors.

Experimental section

Oven-dried glassware was used for all the reactions with magnetic stirring. Thin layer chromatography was performed on silica gel plates coated on aluminum sheets. The TLC spots were visualized under UV light and/or with iodine vapors. All reactions were carried out under an inert atmosphere (nitrogen). All the compounds were purified by column chromatography on silica gel (60–120 mesh). NMR spectra were recorded on a Bruker Avance-III 400 spectrometer with $CDCl_3$ and DMSO-D_6 as solvents and TMS as an internal standard (400 MHz for ^{1}H-NMR and 100 MHz for ^{13}C-NMR). The high-resolution mass spectra (HRMS) were recorded on a Xevo G2-XS QTOF mass spectrometer. Diffraction data were collected using an Xcalibur, Eos, Gemini diffractometer with Cu Kα (λ = 1.54184) and/or Mo Kα (λ = 0.71073) radiation. IR spectra were recorded on a PerkinElmer FTIR RXI spectrometer using KBr pellets. The UV-Visible absorption spectra of all the compounds were measured in chloroform at room temperature on a PerkinElmer Lambda 35 spectrometer using quartz cuvettes and the fluorescence was measured using a Jasco FP-6300 spectrofluorometer. The melting points were recorded in Thiele tubes using paraffin oil and are uncorrected. Solvents and chemicals used were purchased from Spectrochem and Sigma-Aldrich Chemicals Limited, and used without further purification. Dibromobenzochalcogendiazoles **1–3** were synthesized following the literature procedures.[33] Compound **1** was synthesized in four steps starting from *o*-nitroaniline, following the synthetic procedure reported by Yong *et al.*[33a], in an overall yield of 7%. Compounds **2** and **3** were synthesized following the literature procedures reported by Xu *et al.*[33c] in overall yields of 63% and 57%, respectively. The literature reported characterization data[33] were compared with the measured ^{1}H NMR data and melting points to confirm the identity of synthesized compounds **1–3**.

General procedure for the Suzuki–Miyaura reaction (Scheme 1)

An oven dried two neck round bottom flask was charged with dibromobenzochalcogendiazole (0.2 g, 1 eq.), potassium carbonate (4 eq.), and PANI-Pd catalyst (0.12 g, 0.044 mmol of Pd) and the mixture was dissolved in 1,4-dioxane (10 mL). To the reaction mixture phenyl/thiophene boronic acid (2.5 eq.) was added and the mixture was heated at 90–95 °C in an oil bath for 20 h. The reaction mixture was quenched with water and extracted with ethyl acetate (3 × 25 mL). The combined organic phase was washed with water and dried over anhydrous sodium sulfate. The solvent was removed under vacuum and the crude product was purified by column chromatography on silica gel to afford the product.

4,7-Diphenylbenzo[*c*][2,1,3]oxadiazole (4). Yield: 0.17 g (87%); M.P. 188 °C [Lit.[34] 190–191 °C]; ^{1}H-NMR ($CDCl_3$, 400 MHz): δ 7.49–7.52 (m, 1H), 7.54–7.59 (m, 2H), 7.70 (s, 1H), 8.05–8.07 (m, 2H); Mass (EI) *m*/*z*: 272 (M^+, 100), 239 (47). The rest of the characterization data are reported in the literature.[34]

4,7-Diphenylbenzo[*c*][2,1,3]thiadiazole (5). Yield: 0.16 g (83%); M.P. 125 °C [Lit.[35] 127 °C]; ^{1}H-NMR ($CDCl_3$, 400 MHz): δ 7.49–7.51 (m, 1H), 7.56–7.60 (m, 2H), 7.82 (s, 1H), 7.94–8.00 (m, 2H); Mass (EI) *m*/*z*: 289 (M + 1, 100). The rest of the characterization data are reported in the literature.[35]

4,7-Diphenylbenzo[*c*][2,1,3]selenadiazole (6). Yield: 0.16 g (81%); M.P. 175–177 °C [Lit.[28] 177 °C]; ^{1}H-NMR ($CDCl_3$, 400 MHz): δ 7.45–7.549 (m, 1H), 7.54–7.58 (m, 2H), 7.65 (s, 1H), 7.89–7.91 (m, 2H); Mass (EI) *m*/*z*: 355 (M^+, 37), 255 (100), 227 (28). The rest of the characterization data are reported in the literature.[28]

4,7-Di(thiophen-2-yl)benzo[*c*][2,1,3]oxadiazole (7). Yield: 0.16 g (78%); M.P. 121–123 °C [Lit.[29] 123–125 °C]; ^{1}H NMR (400 MHz, $CDCl_3$): δ 7.22–7.24 (m, 2H), 7.46–7.48 (m, 2H), 7.63 (s, 2H), 8.13–8.14 (m, 2H); Mass (EI) *m*/*z*: 284 (M^+, 100), 283 (64), 254 (35). The rest of the characterization data are reported in the literature.[29]

4,7-Di(thiophen-2-yl)benzo[*c*][2,1,3]thiadiazole (8). Yield: 0.16 g (80%); M.P. 123–124 °C [Lit.[36] 123–125 °C]; ^{1}H NMR (400 MHz, $CDCl_3$): δ 7.22–7.24 (m, 2H), 7.47–7.48 (m, 2H), 7.88 (s, 2H), 8.13–8.14 (m, 2H); Mass (EI) *m*/*z*: 300 (M^+, 100), 299 (90). The rest of the characterization data are reported in the literature.[36]

4,7-Di(thiophen-2-yl)benzo[*c*][2,1,3]selenadiazole (9). Yield: 0.14 g (70%); M.P. 126 °C [Lit.[28] 127 °C]; ^{1}H NMR (400 MHz, $CDCl_3$): δ 7.21–7.23 (m, 2H), 7.48–7.49 (m, 2H), 7.82 (s, 2H), 8.03–8.04 (m, 2H); Mass (EI) *m*/*z*: 300 (M^+, 100), 299 (90). The rest of the characterization data are reported in the literature.[28]

General procedure for the Mizoroki–Heck reaction (Scheme 2)

To an oven dried two neck round bottom flask dibromobenzochalcogendiazole **1–3** (0.2 g, 1 eq.), PANI-Pd (0.15 g, 0.055 mmol of Pd) and potassium carbonate (4 eq.) were added. *N*,*N*-Dimethylacetamide (10 mL) was used as the solvent and then styrene **10–12** (2.5 eq.) was added under a nitrogen atmosphere. The reaction mixture was then heated to 120–140 °C in an oil bath for 40 h. The reaction mixture was quenched with water and extracted with ethyl acetate (3 × 50 mL) and dried over anhydrous sodium sulfate. The solvent was removed under vacuum and the crude product was purified by column chromatography on silica gel to afford the product.

4,7-Di((*E*)-styryl)benzo[*c*][2,1,3]oxadiazole (13). Yield: 0.17 g (74%); M.P. 185–186 °C; ^{1}H-NMR (400 MHz, $CDCl_3$): δ 7.29–7.36 (m, 3H), 7.41–7.45 (m, 2H), 7.64–7.66 (m, 2H), 8.06–8.10 (d, ^2J = 16 Hz, 1H); ^{13}C NMR (100 MHz, $CDCl_3$): δ 123.7, 126.2, 127.1, 128.6, 128.8, 130.1, 135.8, 137.0, 148.3; Mass (EI) *m*/*z*: 324 (M^+, 100), 323(73), 295 (44); HRMS (ESI) *m*/*z* calculated for $C_{22}H_{17}N_2O$ $[M + H]^+$ 325.1341, found 325.1332.

4,7-Di((*E*)-styryl)benzo[*c*][2,1,3]thiadi-azole (14). This compound has been reported very recently by Zhang *et al.*[23a] Yield: 0.16 g (71%); M.P. 178 °C; ^{1}H NMR (400 MHz, $CDCl_3$): δ 7.32–7.35 (m, 1H), 7.41–7.45 (m, 2H), 7.66–7.70 (m, 3H), 7.73 (s, 1H), 8.00–8.05 (d, ^2J = 16.4 Hz, 1H); ^{13}C NMR (100 MHz, $CDCl_3$): δ 124.5, 127.0 (2C), 128.1, 128.8, 129.3, 133.2, 137.5, 154.0; Mass (EI) *m*/*z*: 341 (M + 1, 67), 340 (M^+, 100); HRMS (ESI) *m*/*z* calculated for $C_{22}H_{17}N_2S$ $[M + H]^+$ 341.1112, found 341.1111.

4,7-Di((*E*)-styryl)benzo[*c*][2,1,3]selenadiazole (15). Yield: 0.15 g (69%); M.P. 180–181 °C; ^{1}H NMR (400 MHz, $CDCl_3$): δ 7.31–7.34 (m, 1H), 7.40–7.44 (t, ^2J = 8 Hz, 2H), 7.65–7.68 (m, 3H), 7.73–7.77 (d, ^2J = 16.4 Hz, 1H), 7.88–7.93 (d, ^2J = 16.4 Hz, 1H); ^{13}C NMR (100 MHz, $CDCl_3$): δ 124.7, 126.7, 126.9, 128.1, 128.7, 130.8, 132.9, 137.6, 159.6; Mass (EI) *m*/*z*: 387 (M^+ 100), 307 (100); HRMS (ESI) *m*/*z* calculated for $C_{22}H_{17}N_2Se$ $[M + H]^+$ 389.0557, found 389.0555.

4,7-Bis((*E*)-4-methylstyryl)benzo[*c*][2,1,3]oxadiazole (16). Yield: 0.18 g (72%); M.P. 244 °C; ^{1}H NMR (400 MHz, $CDCl_3$): δ 2.41 (s, 3H), 7.23–7.34 (m, 4H), 7.54–7.56 (d, ^2J = 8 Hz, 2H), 8.03–8.07 (d, ^2J = 16 Hz, 1H); ^{13}C NMR (100 MHz, $CDCl_3$): δ 21.4, 122.9, 126.1, 127, 129.5, 130.7, 134.3, 135.7, 138.7, 148.4; HRMS (ESI) *m*/*z* calculated for $C_{24}H_{21}N_2O$ $[M + H]^+$ 353.1654, found 353.1630.

4,7-Bis((*E*)-4-methylstyryl)benzo[*c*][2,1,3]thiadiazole (17). Yield: 0.18 g (73%); M.P. 202 °C; ^{1}H NMR (400 MHz, $CDCl_3$): δ 2.41 (s, 3H), 7.22–7.23 (d, ^2J = 8.4 Hz, 2H), 7.57–7.58 (d, ^2J = 8 Hz, 2H), 7.62–7.66 (d, ^2J = 16.4 Hz, 1H), 7.71 (s, 1H), 7.96–8.00 (d, ^2J = 16.4 Hz, 1H); ^{13}C NMR (100 MHz, $CDCl_3$): δ 21.4, 123.5, 126.7, 126.8, 129.2, 129.5, 133.0, 134.7, 138.1, 154.0; Mass (EI) *m*/*z*: 368 (M^+ 100), 367 (80); HRMS (ESI) *m*/*z* calculated for $C_{24}H_{21}N_2S$ $[M + H]^+$ 369.1425, found 369.1399.

4,7-Bis((*E*)-4-methylstyryl)benzo[*c*][2,1,3]selenadiazole (18). Yield: 0.16 g (65%); M.P. 192–195 °C; ^{1}H NMR (400 MHz, $CDCl_3$): δ 2.40 (s, 3H), 7.22–7.24 (d, ^2J = 8 Hz, 2H), 7.56–7.58 (d, ^2J = 8 Hz, 2H), 7.68–7.72 (d, ^2J = 16.4 Hz, 1H), 7.84–7.88 (d, ^2J = 16.4 Hz, 1H); ^{13}C NMR (100 MHz, $CDCl_3$): δ 21.4, 123.8, 126.5, 126.8, 129.5, 130.7, 132.6, 134.8, 138.1, 159.7; Mass (APCI) *m*/*z*: 417(M + 1), 418(M + 2); HRMS (ESI) *m*/*z* calculated for $C_{24}H_{21}N_2Se$ $[M + H]^+$ 417.0870, found 417.0864.

4,7-Bis((*E*)-2-(pyridin-4-yl)vinyl)benzo[*c*][2,1,3]thiadiazole (19). Yield: 0.07 g (31%); M.P. 225–228 °C [Lit.[5a] 230–232 °C]; ^{1}H NMR (400 MHz, $CDCl_3$): δ 7.52–7.54 (dd, ^2J = 4.8 Hz, ^3J = 1.6 Hz, 2H), 7.78 (s, 1H), 7.79–7.83 (d, ^2J = 16.4 Hz, 1H), 8.04–8.08 (d, ^2J = 16.4 Hz, 1H), 8.65–8.67 (dd, ^2J = 4.8 Hz, ^3J = 1.6 Hz, 2H); ^{13}C NMR (100 MHz, $CDCl_3$): δ 121.1, 128.5, 128.7, 129.3, 131.4, 144.6, 150.3, 153.7; Mass (APCI) *m*/*z*: 343(M + H, 100). The rest of the characterization data are reported in the literature.[5a]

General procedure for the one-pot Wittig–Heck reaction (Scheme 3)

A two neck round bottom flask was charged with dibromobenzothiadiazole **2** (0.2 g, 1 eq.), substituted aldehyde (2.2 eq.), methyl triphenyl phosphonium iodide (2.2 eq.), potassium bicarbonate (12 eq.), and PANI-Pd (0.2 g, 0.073 mmol of Pd) in DMA under a nitrogen atmosphere. This mixture was slowly heated to 120 °C in an oil bath and the heating was continued for 40 h. The reaction mixture was quenched with water and extracted with ethyl acetate (3 × 25 ml). The combined organic phase was washed with water and dried over anhydrous sodium sulphate. The solvent was removed under vacuum and the crude product was purified by column chromatography on silica gel to afford pure products.

4,7-Di((*E*)-styryl)benzo[*c*][2,1,3]thiadiazole (14). This compound has been reported very recently by Zhang *et al.*[23a] Compound **14** was obtained *via* the one-pot Wittig–Heck

methodology with an improved yield compared to that obtained by the standard Mizoroki–Heck reaction. Yield: 0.17 g (74%).

4,7-Bis((*E*)-4-methylstyryl)benzo[*c*][2,1,3]thiadiazole (17). Compound **17** was obtained *via* the one-pot Wittig–Heck methodology with an improved yield compared to that obtained by the standard Mizoroki–Heck reaction. Yield: 0.19 g (75%).

4,7-Bis((*E*)-4-methoxystyryl)benzo[*c*][2,1,3]thiadiazole (20). This compound has been reported very recently by Chen *et al.*[23b] Yield: 0.20 g (74%); M.P. 198–200 °C; ^{1}H NMR (400 MHz, $CDCl_3$): δ 2.41 (s, 3H), 7.23–7.25 (d, ^2J = 8.4 Hz, 2H), 7.57–7.59 (d, ^2J = 8 Hz, 2H), 7.62–7.66 (d, ^2J = 16.4 Hz, 1H), 7.71 (s, 1H), 7.96–8.00 (d, ^2J = 16.4 Hz, 1H); ^{13}C NMR (100 MHz, $CDCl_3$): δ 123.5, 126.7, 126.8, 129.3, 129.5, 133.0, 134.7, 138.1, 153.9; HRMS (ESI) *m*/*z* calculated for $C_{24}H_{21}N_2O_2S$ $[M + H]^+$ 401.1324, found 401.1312.

4,7-Bis((*E*)-2-(benzo[*d*][1,3]dioxol-5-yl)vinyl)benzo[*c*][2,1,3]thiadiazole (21). Yield: 0.19 g (66%); M.P. 190–192 °C; ^{1}H NMR (400 MHz, $CDCl_3$): δ 6.03 (s, 2H), 6.85–6.87 (d, ^2J = 7.6 Hz, 2H), 7.10–7.12 (dd, ^2J = 8.4, ^3J = 1.6 Hz, 2H), 7.23–7.24 (d, ^3J = 1.6 Hz, 1 H) 7.62–7.66 (d, ^2J = 16.4 Hz, 1H), 7.71 (s, 1H), 7.96–8.00 (d, ^2J = 16.4 Hz, 1H); ^{13}C NMR (100 MHz, $CDCl_3$): δ 101.2, 105.7, 108.5, 122.3, 122.9, 126.7, 129.1, 132.1, 132.7, 147.8, 148.3, 153.9; Mass (APCI) *m*/*z*: 429 (M + 1), 430 (M + 2); HRMS (ESI) *m*/*z* calculated for $C_{24}H_{17}N_2O_4S$ $[M + H]^+$ 429.0909, found 429.0906.

4,7-Bis((*E*)-4-chlorostyryl)benzo[*c*][2,1,3]thiadiazole (22). Yield: 0.18 g (65%); M.P. 256–258 °C; ^{1}H NMR (400 MHz, $CDCl_3$): δ 7.38–7.40 (m, 2H), 7.60–7.64 (m, 4H), 7.70 (s, 1H), 7.99–8.03 (d, ^2J = 16.4 Hz, 1H); ^{13}C NMR (100 MHz, $CDCl_3$): δ 125.0, 127.3, 128.1, 129.0, 129.2, 132.1, 133.8, 135.9, 153.7; HRMS (ESI) *m*/*z* calculated for $C_{22}H_{15}Cl_2N_2S$ $[M + H]^+$ 409.0255, found 408.9804.

4,7-Bis((*E*)-4-fluorostyryl)benzo[*c*][2,1,3]thiadiazole (23). Yield: 0.17 g (66%); M.P. 235–237 °C; ^{1}H NMR (400 MHz, $CDCl_3$): δ 7.01–7.14 (t, ^2J = 8.8 Hz, 2H), 7.55–7.59 (d, ^2J = 16.4 Hz, 1H), 7.63–7.66 (m, 2H), 7.70 (s, 1H), 7.98–8.02 (d, ^2J = 16.4 Hz, 1H); ^{13}C NMR (100 MHz, $CDCl_3$): δ 115.7–115.9 (d, $^3J_{CF}$ = 21 Hz, 2C), 124.3, 127.0, 128.4–128.5 (d, $^4J_{CF}$ = 8 Hz, 2C), 129.2, 132.1, 132.6, 153.9, 161.4–163.9 (d, $^2J_{CF}$ = 247 Hz); Mass (APCI) *m*/*z*: 377(M + 1), 378(M + 2); HRMS (ESI) *m*/*z* calculated for $C_{22}H_{15}F_2N_2S$ $[M + H]^+$ 377.0924, found 377.0912.

4,4′-((1*E*,1′*E*)-Benzo[*c*][2,1,3]thiadiazole-4,7-diylbis(ethene-2,1-diyl))dibenzonitrile (24). Yield: 0.17 g (64%); M.P. 270–272 °C; ^{1}H NMR (400 MHz, $CDCl_3$): δ 7.70–7.76 (m, 6H), 8.10–8.15 (d, ^2J = 16.4 Hz, 1H); ^{13}C NMR (100 MHz, $CDCl_3$): δ 111.2, 118.9, 127.3, 127.9, 128.2, 129.3, 132.0, 132.6, 141.8, 153.8; HRMS (ESI) *m*/*z* calculated for $C_{24}H_{15}N_4S$ $[M + H]^+$ 391.1012, found 391.1015.

4,7-Bis((*E*)-4-nitrostyryl)benzo[*c*][2,1,3]thiadiazole (25). Yield: 0.18 g (60%); M.P. 220–222 °C; ^{1}H NMR (400 MHz, $CDCl_3$): δ 7.75–7.79 (d, ^2J = 16.4 Hz, 1H), 7.79–7.82 (m, 3H), 8.19–8.23 (d, ^2J = 16.4 Hz, 1H), 8.29–8.31 (m, 2H); ^{13}C NMR (100 MHz, $CDCl_3$): δ 124.3, 127.4, 128.6, 129.4, 131.8, 131.9, 143.8, 149.5, 153.7; HRMS (ESI) *m*/*z* calculated for $C_{22}H_{14}N_4O_4S$ [M+] 430.0730, found 430.0703.

Conflicts of interest

There are no conflicts to declare.

Acknowledgements

We thank the University Grants Commission (UGC), New Delhi for the financial support (F No 42-240/2013). VJB wish to thanks UGC-BSR for providing financial assistance (No. F.4-1/2006(BSR)/7-303/2010(BSR)). ALP also wishes to thank the Research and Consultancy Cell-MSU Baroda for financial assistance (No RCC/Dir./2017/335/15). The authors would like to acknowledge the DST-FIST program for funding the NMR facility at the Department of Chemistry and the DST-PURSE program for the single crystal X-ray diffractometer facility at the Faculty of Science, M. S. University of Baroda.

References

1 (*a*) M. Karikomi, C. Kitamura, S. Tanaka and Y. Yamashita, *J. Am. Chem. Soc.*, 1995, **117**, 6791–6792; (*b*) Y. Yamashita, K. Suzuki and M. Tomura, *Synth. Met.*, 2003, **133–134**, 341–343; (*c*) B. A. DaSilveira Neto, A. S. A. Lopes, G. Ebeling, R. S. Gonçalves, V. E. U. Costa, F. H. Quina and J. Dupont, *Tetrahedron*, 2005, **61**, 10975–10982.

2 (*a*) Y. Yang, Y. Zhou, Q. He, C. He, C. Yang, F. Bai and Y. Li, *J. Phys. Chem. B*, 2009, **113**, 7745–7752; (*b*) H. Li, Z. Chi, X. Zhang, B. Xu, S. Liu, Y. Zhang and J. Xu, *Chem. Commun.*, 2011, **47**, 11273–11275.

3 (*a*) A. Dhanabalan, J. K. J. van Duren, P. A. van Hal, J. L. J. van Dongen and R. A. J. Janssen, *Adv. Funct. Mater.*, 2001, **11**, 255–262; (*b*) A. Distler, P. Kutka, T. Sauermann, H.-J. Egelhaaf, D. M. Guldi, D. Di Nuzzo, S. C. J. Meskers and R. A. J. Janssen, *Chem. Mater.*, 2012, **24**, 4397–4405; (*c*) X. Cheng, Y.-Y. Noh, J. Wang, M. Tello, J. Frisch, R.-P. Blum, A. Vollmer, J. P. Rabe, N. Koch and H. Sirringhaus, *Adv. Funct. Mater.*, 2009, **19**, 2407–2415.

4 (*a*) M. Horie, J. Kettle, C.-Y. Yu, L. A. Majewski, S.-W. Chang, J. Kirkpatrick, S. M. Tuladhar, J. Nelson, B. R. Saunders and M. L. Turner, *J. Mater. Chem.*, 2012, **22**, 381–389; (*b*) P. B. Pati, S. P. Senanayak, K. S. Narayan and S. S. Zade, *ACS Appl. Mater. Interfaces*, 2013, **5**, 12460–12468.

5 (*a*) M. N. K. Prasad Bolisetty, C.-T. Li, K. R. J. Thomas, G. B. Bodedla and K.-C. Ho, *Tetrahedron*, 2015, **71**, 4203–4212; (*b*) H. Padhy, J.-H. Huang, D. Sahu, D. Patra, D. Kekuda, C.-W. Chu and H.-C. Lin, *J. Polym. Sci., Part A: Polym. Chem.*, 2010, **48**, 4823–4834.

6 (*a*) T. Ishi-I, M. Sakai and C. Shinoda, *Tetrahedron*, 2013, **69**, 9475–9480; (*b*) X. Zhang, H. Gorohmaru, M. Kadowaki, T. Kobayashi, T. Ishi-i, T. Thiemann and S. Mataka, *J. Mater. Chem.*, 2004, **14**, 1901–1904; (*c*) T. Ishi-i, N. Nakamura, N. Esaki and S. Amemori, *Chem. Lett.*, 2008, **37**, 1166–1167; (*d*) T. Ishi-i, N. Nakamura, T. Mine, S. Imamura, M. Shigeiwa, H. Gorohmaru and S. Maeda, *Chem. Lett.*, 2009, **38**, 1042–1043.

7 (*a*) Y. Lei, H. Li, W. Gao, M. Liu, J. Chen, J. Ding, X. Huang and H. Wu, *J. Mater. Chem. C*, 2014, **2**, 7402–7410; (*b*) X. Huang, J. Meng, Y. Dong, Y. Cheng and C. Zhu, *J. Polym. Sci., Part A: Polym. Chem.*, 2010, **48**, 997–1006.

8 (*a*) L. Chen, L. Wang, X. Jing and F. Wang, *J. Mater. Chem.*, 2011, **21**, 10265–10267; (*b*) G. L. Gibson, T. M. McCormick and D. S. Seferos, *J. Am. Chem. Soc.*, 2012, **134**, 539–547; (*c*) D. Li, H. Li, M. Liu, J. Chen, J. Ding, X. Huang and H. Wu, *Macromol. Chem. Phys.*, 2014, **215**, 82–89.

9 (*a*) D. S. Chung, H. Kong, W. M. Yun, H. Cha, H.-K. Shim, Y.-H. Kim and C. E. Park, *Org. Electron.*, 2010, **11**, 899–904; (*b*) J.-M. Jiang, P. Raghunath, H.-K. Lin, Y.-C. Lin, M. C. Lin and K.-H. Wei, *Macromolecules*, 2014, **47**, 7070–7080; (*c*) Z. Liu, J. He, H. Zhuang, H. Li, N. Li, D. Chen, Q. Xu, J. Lu, K. Zhang and L. Wang, *J. Mater. Chem. C*, 2015, **3**, 9145–9153; (*d*) S. Haid, A. Mishra, C. Uhrich, M. Pfeiffer and P. Bäuerle, *Chem. Mater.*, 2011, **23**, 4435–4444.

10 (*a*) K. Ono, S. Tanaka and Y. Yamashita, *Angew. Chem., Int. Ed. Engl.*, 1994, **33**, 1977–1979; (*b*) Y. Yamashita, K. Ono, M. Tomura and K. Imaeda, *Chem. Commun.*, 1996, 2021–2022; (*c*) Y. Yamashita, K. Ono, M. Tomura and K. Imaeda, *Chem. Commun.*, 1997, 1851–1852.

11 (*a*) B. D. Lindner, B. A. Coombs, M. Schaffroth, J. U. Engelhart, O. Tverskoy, F. Rominger, M. Hamburger and U. H. F. Bunz, *Org. Lett.*, 2013, **15**, 666–669; (*b*) A. F. Cozzolino and I. Vargas-Baca, *Cryst. Growth Des.*, 2011, **11**, 668–677; (*c*) S. Tsuzuki and N. Sato, *J. Phys. Chem. B*, 2013, **117**, 6849–6855; (*d*) Y. Yi, H. Xu, L. Wang, W. Cao and X. Zhang, *Chem. – Eur. J.*, 2013, **19**, 9506–9510.

12 R. F. Heck and J. P. Nolley, *J. Org. Chem.*, 1972, **37**, 2320–2322.

13 (*a*) A. Suzuki, *J. Organomet. Chem.*, 1999, **576**, 147–168; (*b*) N. Miyaura and A. Suzuki, *J. Chem. Soc., Chem. Commun.*, 1979, 866–867.

14 C. Kitamura, S. Tanaka and Y. Yamashita, *Chem. Mater.*, 1996, **8**, 570–578.

15 A. Biffis, M. Zecca and M. Basato, *J. Mol. Catal. A: Chem.*, 2001, **173**, 249–274.

16 (*a*) T. Punniyamurthy and J. Iqbal, *Tetrahedron Lett.*, 1997, **38**, 4463–4466; (*b*) S. Das and T. Punniyamurthy, *Tetrahedron Lett.*, 2003, **44**, 6033–6035; (*c*) J. G. Handique, L. Borah, R. J. Sarma and J. B. Baruah, *J. Mol. Catal. A: Chem.*, 2002, **188**, 63–69; (*d*) B. C. Das and J. Iqbal, *Tetrahedron Lett.*, 1997, **38**, 1235–1238; (*e*) S. Velusamy and T. Punniyamurthy, *Org. Lett.*, 2004, **6**, 217–219; (*f*) J. P. Nandy, E. N. Prabhakaran, S. K. Kumar, A. C. Kunwar and J. Iqbal, *J. Org. Chem.*, 2003, **68**, 1679–1692; (*g*) J. Haber, M. Kłosowski and J. Połtowicz, *J. Mol. Catal. A: Chem.*, 2003, **201**, 167–178.

17 P. R. Likhar, R. Arundhathi, S. Ghosh and M. L. Kantam, *J. Mol. Catal. A: Chem.*, 2009, **302**, 142–149.

18 (*a*) M. L. Kantam, M. Roy, S. Roy, B. Sreedhar, S. S. Madhavendra, B. M. Choudary and R. L. De, *Tetrahedron*, 2007, **63**, 8002–8009; (*b*) Y. Chen, S. Lu, W. Liu and J. Han, *Colloid Polym. Sci.*, 2015, **293**, 2301–2309.

19 (*a*) B. M. Choudary, M. Roy, S. Roy, M. L. Kantam, B. Sreedhar and K. V. Kumar, *Adv. Synth. Catal.*, 2006, **348**, 1734–1742; (*b*) S. Palaniappan and R. Chandra Shekhar, *J. Mol. Catal. A: Chem.*, 2004, **209**, 117–124; (*c*) M. He, C. Lie, G. Luo and C. Wang, *Polym.-Plast. Technol. Eng.*, 2007, **46**, 145–149; (*d*) A. L. Patel, H. R. Talele, H. S. Rama and A. V. Bedekar, *Synth. Commun.*, 2009, **39**, 3016–3023.

20 (*a*) H. A. Patel, A. L. Patel and A. V. Bedekar, *Appl. Organomet. Chem.*, 2015, **29**, 1–6; (*b*) H. A. Patel, A. M. Sawant, V. J. Rao, A. L. Patel and A. V. Bedekar, *Catal. Lett.*, 2017, **147**, 2306–2312; (*c*) H. A. Patel, A. L. Patel and A. V. Bedekar, *New J. Chem.*, 2016, **40**, 8935–8945; (*d*) H. A. Patel, M. Rawat, A. L. Patel and A. V. Bedekar, *Appl. Organomet. Chem.*, 2019, **33**, e4767.

21 (*a*) A. S. Saiyed and A. V. Bedekar, *Tetrahedron Lett.*, 2010, **51**, 6227–6231; (*b*) K. N. Patel and A. V. Bedekar, *Tetrahedron Lett.*, 2015, **56**, 6617–6621.

22 (*a*) S. J. Broadwater, S. L. Roth, K. E. Price, M. Kobašlija and D. T. McQuade, *Org. Biomol. Chem.*, 2005, **3**, 2899–2906; (*b*) J. M. Lee, Y. Na, H. Han and S. Chang, *Chem. Soc. Rev.*, 2004, **33**, 302–312.

23 (*a*) J. Zhang, A. Konsmo, A. Sandberg, X. Wu, S. Nystrom, U. Obermuller, B. M. Wegenast-Braun, P. Konradsson, M. Lindgren and P. Hammarstrom, *J. Med. Chem.*, 2019, **62**, 2038–2048; (*b*) J. Chen, F. Ye, Y. Lin, Z. Chen, S. Liu and J. Yin, *Sci. China: Chem.*, 2019, **62**, 440–450.

24 E. N. Prabhakaran and J. Iqbal, *J. Org. Chem.*, 1999, **64**, 3339–3341.

25 B. A. Coombs, B. D. Lindner, R. M. Edkins, F. Rominger, A. Beeby and U. H. F. Bunz, *New J. Chem.*, 2012, **36**, 550–553.

26 (*a*) Y. Il Park, C.-Y. Kuo, J. S. Martinez, Y.-S. Park, O. Postupna, A. Zhugayevych, S. Kim, J. Park, S. Tretiak and H.-L. Wang, *ACS Appl. Mater. Interfaces*, 2013, **5**, 4685–4695; (*b*) A. J. Zucchero, J. N. Wilson and U. H. F. Bunz, *J. Am. Chem. Soc.*, 2006, **128**, 11872–11881.

27 P. Blanchard, J.-M. Raimundo and J. Roncali, *Synth. Met.*, 2001, **119**, 527–528.

28 P. B. Pati and S. S. Zade, *Cryst. Growth Des.*, 2014, **14**, 1695–1700.

29 P. B. Pati, S. Das and S. S. Zade, *J. Polym. Sci., Part A: Polym. Chem.*, 2012, **50**, 3996–4003.

30 R. Ganduri, S. Cherukuvada, S. Sarkar and T. N. Guru Row, *CrystEngComm*, 2017, **19**, 1123–1132.

31 B. R. Bhogala, S. Basavoju and A. Nangia, *CrystEngComm*, 2005, **7**, 551–562.

32 (*a*) C. B. Aakeröy, J. Desper and J. F. Urbina, *Chem. Commun.*, 2005, 2820–2822; (*b*) Y.-H. Luo and B.-W. Sun, *Spectrochim. Acta, Part A*, 2014, **120**, 228–236.

33 (*a*) L. Q. Yong, Q. Yong, L. Jianren, L. Yinkui and G. Yudi, *Chinese Pat.*, CN200510135385 20051231, 2006; (*b*) D. Wen, Y. Y. Fu, L. Q. Shi, C. He, L. Dong, D. F. Zhu, Q. G. He, H. M. Cao and J. G. Cheng, *Sens. Actuators, B*, 2012, **168**, 283–288; (*c*) S. Xu, Y. Liu, J. Li, Y. Wang and S. Cao, *Polym. Adv. Technol.*, 2010, **21**, 663–668.

34 I. Idris, F. Derridj, J.-F. Soulé and H. Doucet, *Adv. Synth. Catal.*, 2017, **359**, 2448–2456.

35 F. S. Mancilha, B. A. DaSilveira Neto, A. S. Lopes, P. F. Moreira Jr., F. H. Quina, R. S. Gonçalves and J. Dupont, *Eur. J. Org. Chem.*, 2006, **2006**, 4924–4933.

36 S. Mattiello, M. Rooney, A. Sanzone, P. Brazzo, M. Sassi and L. Beverina, *Org. Lett.*, 2017, **19**, 654–657.

